Systematics of c-axis phonons in the thallium- and bismuth-based cuprate superconductors

A. A. Tsvetkov

Laboratory of Solid State Physics, Materials Science Center, Groningen University, Nijenborgh 4, 9747 AG Groningen, The Netherlands
and P. N. Lebedev Physical Institute, Russian Academy of Sciences, Leninsky Prospect 53, 117924 Moscow, Russia

D. Dulić, D. van der Marel, and A. Damascelli

Laboratory of Solid State Physics, Materials Science Center, Groningen University, Nijenborgh 4, 9747 AG Groningen, The Netherlands

G. A. Kaljushnaia, J. I. Gorina, and N. N. Senturina

P. N. Lebedev Physical Institute, Russian Academy of Sciences, Leninsky Prospect 53, 117924 Moscow, Russia

N. N. Kolesnikov

Institute of Solid State Physics, Russian Academy of Sciences, Chernogolovka 142432, Russia

Z. F. Ren and J. H. Wang

Department of Chemistry, SUNY at Buffalo, Buffalo, New York 14260-3000

A. A. Menovsky

Van der Waals–Zeeman Laboratory, University of Amsterdam, Amsterdam, The Netherlands

T. T. M. Palstra

Inorganic Solid State Chemistry Laboratory, Materials Science Center, Groningen University, Nijenborgh 4,
9747 AG Groningen, The Netherlands

(Received 20 January 1999)

We present grazing incidence reflectivity measurements in the far-infrared region at temperatures above and below T_c for a series of thallium- ($Tl_2Ba_2CuO_6$, $Tl_2Ba_2CaCu_2O_8$) and bismuth- ($Bi_2Sr_2CuO_6$, $Bi_2Sr_2CaCu_2O_8$, and $Bi_{2-x}Pb_xSr_2CaCu_2O_8$) based cuprate superconductors. From the spectra, which are dominated by the c-axis phonons, longitudinal optical (LO) frequencies are directly obtained. The reflectivity curves are well fitted by a series of Lorentz oscillators. In this way the transverse optical (TO) phonon frequencies were accurately determined. On the basis of the comparative study of the Bi- and Tl-based cuprates with a different number of CuO_2 layers per unit cell, we suggest modifications of the assignment of the main oxygen modes. We compare the LO frequencies in $Bi_2Sr_2CaCu_2O_8$ and $Tl_2Ba_2Ca_2Cu_3O_{10}$ obtained from intrinsic Josephson junction characteristics with our measurements, and explain the discrepancy in LO frequencies obtained by the two different methods. [S0163-1829(99)04938-3]

I. INTRODUCTION

The phonon spectra of high-temperature superconductors were widely studied due to the possible important role in the mechanism of superconductivity. Besides that, the phonons being on the same energy scale as the superconducting gap strongly affected many superconductivity-related quantities, such as electronic response and the superconducting energy gap, pseudogap, Josephson plasma oscillations, and tunneling spectra. The first optical measurements were performed on polycrystalline samples.[1] The assignment of the phonon modes and the lattice dynamical calculations used for the assignment were strongly influenced by the mixed in-plane and out-of-plane response in these earlier data. As large single crystals became available, the infrared (IR) properties and, in particular, the c-axis phonons of the yttrium- and lanthanum-based compounds were thoroughly investigated, providing phonon eigenvector patterns[2–5] different from the early assignment. The c-axis response of the bismuth and thallium classes of superconductors is known to a much

lesser extent. The measurements done on these materials probed primarily the ab properties,[6–9] or polycrystalline samples were used.[10–14] Unambiguous information on the IR c-axis phonon spectra was obtained on $Bi_2Sr_2CaCu_2O_8$ (Bi2212) single crystals[15,16] and on $Tl_2Ba_2Ca_2Cu_3O_{10}$ (Tl2223) film.[17] Extensive studies, along with efforts to assign the main oxygen modes in these compounds were also performed using Raman scattering.[18–29]

In this paper we present a systematic study of the c-axis IR phonons in Bi and Tl cuprates by means of grazing angle reflectivity measurements. We discuss the technique used and show its sensitivity to the c-axis properties in anisotropic materials. The comparison with the available data on Bi2212 by Tajima *et al.*[16] proves that both transverse optical (TO) and longitudinal optical (LO) c-axis frequencies can be determined correctly by this method. We report on measurements of the c-axis vibrational spectra in single-layer Bi and Tl compounds, done on single crystals. By comparing bismuth and thallium compounds with the different number of CuO_2 layers per unit cell (single- and double-layer systems),

we propose a consistent assignment of the main oxygen modes, different from those done by lattice dynamical calculations.[30,31] In the bismuth cuprate, using lead-doped samples, we identify the superstructure-induced modes. The particular sensitivity of our technique to the longitudinal modes enables a direct comparison of our data to the fine structure observed in the intrinsic Josephson junction characteristics,[32,33] which was ascribed to the LO phonon excitations.[34]

II. EXPERIMENT

The reflectivity measurements were performed at a grazing angle of 80° relative to the surface normal, with p-polarized light (electric vector in the plane of incidence), in the far-infrared (FIR) region (30–700 cm^{-1}). Reference spectra were obtained by evaporating a gold film *in situ* on the sample surface, and absolute reflectivities were determined by the reflectivity ratio. A wire grid polarizer was used to select the proper polarization. The measurements were made using a Fourier transform spectrometer (Bruker IFS 113v). A series of samples was measured.

$Bi_2Sr_2CuO_6$ (Bi2201), $Bi_2Sr_2CaCu_2O_8$ (Bi2212), and lead-doped $Bi_{2-x}Pb_xSr_2CaCu_2O_8$ (Bi2212+Pb) single crystals were grown at the Lebedev Physical Institute by the method of recrystallization from the precursor dissolved in melted KCl.[35–37] As-grown samples were obtained as freestanding thin crystalline platelets and did not require any further treatment. The transition temperatures (and the transition widths) were $T_c = 6–8$ K ($\Delta T_c = 2$ K), $T_c = 80$ K ($\Delta T_c = 2$ K), and $T_c = 75$ K ($\Delta T_c = 3$ K), respectively. The lead content in the doped samples was $x = 0.4$, as determined by the x-ray electron probe microanalysis.

$Bi_2Sr_2CaCu_2O_8$ single crystals of a larger size (3×4 mm^2) were grown at the University of Amsterdam by the traveling solvent floating zone method.[38] The transition temperature and the transition width were $T_c = 89$ K and $\Delta T_c = 3$ K, respectively. An optically clean surface was obtained by peeling the samples along the ab plane.

$Tl_2Ba_2CuO_6$ (Tl2201) single crystals were produced at the Institute of Solid State Physics. The samples, with $T_c = 82$ K and $\Delta T_c = 13$ K, were obtained by the self-flux method.[39,40]

$Tl_2Ba_2CuO_6$ films came from SUNY at Buffalo. They were made by radio-frequency magnetron sputtering followed by post-deposition annealing.[41] The films had $T_c = 80$ K. More details on the preparation and properties of the films can be found in Refs. 41 and 42.

$Tl_2Ba_2CaCu_2O_8$ (Tl2212) films were provided by Superconductor Technologies Inc. and were produced using their standard production methods[43] and had $T_c = 98$ K. More details on the electrical properties of these films can be found in Ref. 44.

The samples were mounted in a conventional liquid He flow optical cryostat, which allowed any temperature, between room temperature and 8 K, to be reached.

III. TECHNIQUE

The geometry of the grazing angle technique is shown in the inset of Fig. 1, below. From the figure it is easy to see that s-polarized light probes the ab-plane properties of a crystal, whereas p polarization gives much information about the c-axis response. This is a convenient method for extracting both the ab-plane ($\varepsilon_{ab} = \varepsilon'_{ab} + i\varepsilon''_{ab} = n^2_{ab}$), and the c-axis ($\varepsilon_c = \varepsilon'_c + i\varepsilon''_c$) components of the dielectric tensor, in case normal incidence measurements on the ac plane are not possible due to the small size of samples along the c axis or to the mica like nature of the Bi compounds. All cuprate superconductors are highly anisotropic in the ac or bc planes. The ab-plane anisotropy is much smaller. It does not affect our analysis and is neglected in the following discussion. In this case the reflectivity R_p is described by the Fresnel formula for a uniaxial crystal:

$$R_p = \left| \frac{\sqrt{\varepsilon_{ab}} \cos\theta - \sqrt{1 - \dfrac{\sin^2\theta}{\varepsilon_c}}}{\sqrt{\varepsilon_{ab}} \cos\theta + \sqrt{1 - \dfrac{\sin^2\theta}{\varepsilon_c}}} \right|^2, \quad (1)$$

where θ is the angle of incidence, in this case equal to 80°. In order to fit the data, we need to assume a form for ε_{ab} and ε_c. The most common procedure is to use the Drude or two-fluid model (in case of a superconductor):

$$\varepsilon_{ab,c}(\omega) = \varepsilon^{ab,c}_\infty - \frac{\omega^2_{p_{ab,c}}}{\omega^2} + \frac{4\pi i \sigma_{ab,c}}{\omega} + \sum_j \frac{S_j \omega^2_{T_j}}{\omega^2_{T_j} - \omega^2 - i\omega\gamma_j}, \quad (2)$$

where the first term represents high-energy interband transitions, the second and the third terms are superconducting and normal carrier responses, respectively, and the last one is a sum of phonon contributions. In the normal state, the electronic background largely affects ε_{ab}, since the ab planes are metallic, whereas the c-axis properties are insulator like. This means that the most prominent phonon modes are polarized along the c axis, with the ab-plane phonons being strongly screened by the free carriers. The reflectivity function R_p has sharp minima when ε'_c goes to zero, i.e., at the longitudinal frequencies, while the general trend depends on ε_{ab}. The phonons associated with the ab plane are much broader and almost absent in the spectra, so we can assume that ε_{ab} is a smooth function of frequency.

The advantage of the grazing angle technique is that the c-axis longitudinal frequencies are determined directly from the measured data, without any modeling.[45,46] From the reflectivity we can calculate a pseudoloss function $L(\omega)$, defined as[47]

$$L(\omega) = \frac{(1 - R_p)|n_{ab}|\cos\theta}{2(1 + R_p)} \sim \mathrm{Im}\, e^{i\phi} \sqrt{1 - \frac{\sin^2\theta}{\varepsilon_c}}, \quad (3)$$

where n_{ab} is the in-plane complex refraction index and $\phi = \pi/2 - \arg(n_{ab})$ is a weakly frequency-dependent phase shift. $L(\omega)$ is approximately the same as the c-axis loss function $\mathrm{Im}(-1/\varepsilon_c)$ (at least the maxima of both functions are at the same positions), and it gives us the frequencies of the c-axis longitudinal phonons. The reason for observing the LO phonon (and not TO) frequencies in R_p is common for the c-axis plasmon[48] and phonons, and is the following:

The incident electromagnetic radiation excites a wave inside the material, which has an electric field component $\vec{\mathbf{E}} = \vec{\mathbf{E}}e^{i(\vec{\mathbf{k}}\cdot\vec{\mathbf{r}}-\omega t)}$, where each component of $\vec{E}$ and $\vec{k}$ can be complex. If the x axis lies at the intersection of the plane of incidence with the surface, and the z axis is normal to the surface, then the x component of the wave vector, k_x, is determined by the incident radiation, while the z component of the wave vector can be shown to depend both on the in-plane and out-of-plane dielectric functions, as follows:

$$k_x = \frac{\omega}{c}\sin\theta, \quad k_z^2 = \frac{\omega^2}{c^2}\varepsilon_{ab}\left(1 - \frac{\sin^2\theta}{\varepsilon_c}\right), \quad (4)$$

where ω is the frequency of incident radiation and c is the speed of light. Inside the medium the wave remains polarized in the xz plane, and the components of electric field relate to each other as

$$\frac{E_z}{E_x} = \frac{\sqrt{\varepsilon_{ab}}}{\sqrt{\varepsilon_c - \sin^2\theta}}. \quad (5)$$

This illustrates the well-known fact that the electromagnetic wave in an anisotropic medium does not have a pure transverse character, but it has also a longitudinal component, unless it propagates along the principal axes.

In most high-T_c compounds the c-axis plasma frequency is far below the optical phonon frequencies and the phonon modes are well separated in frequency, while the in-plane response is mostly dominated by plasma oscillations of carriers in the ab plane. Thus, the dielectric function $\varepsilon_{ab}(\omega)$ at low frequencies can be written as a pure plasma response, and $\varepsilon_c(\omega)$ near a particular phonon can be simplified to a single Lorentz oscillator:

$$\varepsilon_{ab}(\omega) = \varepsilon_\infty^{ab} - \frac{\omega_{pab}^2}{\omega^2}, \quad \varepsilon_c(\omega) = \varepsilon_{sc} + \frac{S\omega_T^2}{\omega_T^2 - \omega^2}, \quad (6)$$

where ω_{pab} is the in-plane plasma frequency, ω_T is the TO phonon frequency, S is the oscillator strength, and ε_{sc} includes also contribution to ε_∞ from other phonons. In both functions, we neglect the damping for simplicity.

The substitution of Eqs. (6) into Eqs. (4) gives a pure imaginary solution for $k_z(\omega)$ everywhere, except for a narrow frequency range, where ω^2 varies between $\omega_L^2 = \omega_T^2 + S\omega_T^2/\varepsilon_{sc}$ and $\omega_T^2 + S\omega_T^2/(\varepsilon_{sc} - \sin^2\theta)$. In this region $k_z(\omega)$ is real. This corresponds to the propagation of a traveling electromagnetic wave in the medium, which reduces the reflectivity. Outside this narrow frequency range the electromagnetic wave decays exponentially near the surface, and the total reflection takes place. The finite scattering rate in the planes gives rise to the Hagen-Rubens behavior of the reflectivity, while the phonon damping and the c-axis conductivity determine the width of the phonon lines.

IV. RESULTS

The room temperature spectra of Bi2201, Bi2212, Bi2212+Pb, Tl2201, and Tl2212 are shown in Fig. 1. The solid lines represent the fit, and the symbols are the experimental data. These results were reproduced on a number of Bi and Tl samples. The data were collected at temperatures
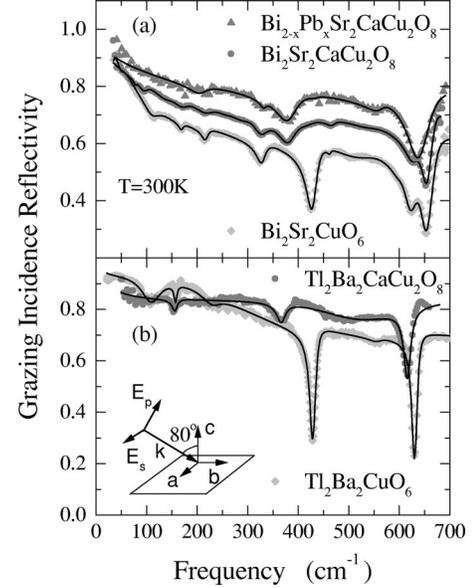

FIG. 1. Experimental (symbols) and fitted (solid lines) grazing angle reflectivity R_p for the p-polarized light measured at an 80° angle of incidence at room temperature for (a) bismuth and (b) thallium compounds. Sketched in the inset is the schematic diagram of the grazing angle technique.

between 8 K and 300 K. The main temperature variations in R_p occur due to the changes in the in-plane response. Bi compounds show more optical phonons due to the lower symmetry. For all five compounds, the overall reflectivity scales with the in-plane response. In general, the double-layer compounds have higher conductivity in the plane than the corresponding single-layer compounds and, consequently, they have higher reflectivity. The optical conductivity of Tl cuprates usually is at least twice as high as that of Bi. The reflectivity R_p was fitted with Eq. (1) and Eq. (2). The fitting parameters—TO frequencies, oscillator strengths S_j, and the damping parameters γ_j of the phonons—as well as LO frequencies (obtained as the positions of maxima in the loss function) are listed in Table I and Table II. The temperature dependence of the phonon parameters can be seen from the comparison to the 8 K data, shown in the

TABLE I. c-axis phonon parameters of the Tl2201 and Tl2212 at room temperature. The values between the parentheses were obtained at 8 K, $\varepsilon_\infty = 4$.

$\tilde{\nu}_{T_j}$ [cm^{-1}]	$\tilde{\nu}_{L_j}$ [cm^{-1}]	γ_j [cm^{-1}]	S_j
Tl$_2$Ba$_2$CuO$_6$			
77.9 (77.9)	111.0 (111.3)	26.5 (26.5)	4.5 (4.5)
156.5 (156.0)	158.0 (157.8)	8.6 (6.1)	0.12 (0.11)
385.5 (385.7)	427.1 (426.7)	8.3 (6.5)	0.94 (0.95)
603.2 (603.3)	628.3 (628.5)	8.7 (8.6)	0.28 (0.28)
Tl$_2$Ba$_2$CaCu$_2$O$_8$			
152.0 (152.0)	156.4 (157.0)	12.2 (9.0)	0.13 (0.13)
339.0 (339.0)	366.3 (367.0)	20.8 (18.0)	1.02 (1.10)
598.1 (602.0)	614.7 (617.0)	17.1 (12.0)	0.22 (0.23)

TABLE II. c-axis phonon parameters of the Bi2201 and Bi2212 at 300K (8 K), $\varepsilon_\infty = 4$.

	Bi$_2$Sr$_2$CuO$_6$		
$\tilde{\nu}_{T_j}$ [cm^{-1}]	$\tilde{\nu}_{L_j}$ [cm^{-1}]	γ_j [cm^{-1}]	S_j
83.0 (87.0)	118.3 (115.6)	15.0 (12.0)	0.35 (0.36)
144.5 (148.7)	169.7 (175.0)	11.0 (11.0)	0.70 (0.68)
196.4 (198.3)	217.2 (218.0)	16.0 (12.1)	0.68 (0.60)
292.0 (307.4)	328.4 (329.8)	25.0 (21.7)	1.20 (1.02)
381.0 (390.5)	426.8 (427.0)	12.5 (10.8)	0.65 (0.62)
461.6 (461.8)	462.6 (462.8)	10.0 (8.0)	0.002 (0.002)
583.8 (595.7)	622.5 (626.1)	24.5 (22.0)	0.46 (0.41)
638.9 (643.8)	652.2 (654.5)	16.4 (11.5)	0.04 (0.04)

		Bi$_2$Sr$_2$CaCu$_2$O$_8$			
$\tilde{\nu}_{T_j}$	$\tilde{\nu}_{L_j}$	γ_j	S_j	$\tilde{\nu}_{T_j}$[a]	$\tilde{\nu}_{L_j}$[b]
81.0	96.7	15.0	0.80		
(77.9)	(94.8)	(12.0)	(0.76)	95	97
157.2	173.5	34.4	0.59		
(160.0)	(177.4)	(30.1)	(0.32)	173	175
198.3	220.0	35.3	0.79		
(200.0)	(222.0)	(35.0)	(0.70)	210	218
301.2	328.4	33.0	0.88		
(325.0)	(330.6)	(16.2)	(0.98)	312	327
356.9	383.0	49.7	0.21		
(365.0)	(372.9)	(28.9)	(1.02)	359	380
461.7	468.7	7	0.001		
(465.0)	(467)	(2.1)	(0.001)	468	470
470.2	472.3	10	0.003		
(478.0)	(480)	(5.0)	(0.003)		
610.0	627.7	28.7	0.23		
(613.5)	(631.1)	(27.0)	(0.22)	580	630
638.5	655.1	13.0	0.05		
(646.9)	(655.9)	(12.9)	(0.05)	622	675

Bi$_{2-x}$Pb$_x$Sr$_2$CaCu$_2$O$_8$			
$\tilde{\nu}_{T_j}$ [cm^{-1}]	$\tilde{\nu}_{L_j}$ [cm^{-1}]	γ_j [cm^{-1}]	S_j
192.8	208.0	43.8	1.22
305.3	332.5	15.8	1.37
350.0	380.2	29.8	0.34
593.5	635.7	28.1	0.72

[a]Positions of maxima in ε'', from Tajima $et\ al.$ (Ref. 16).
[b]Positions of maxima in the loss function, from Tajima $et\ al.$ (Ref. 16).

brackets. The c-axis conductivities and loss functions calculated from the fit are shown in Fig. 2 and Fig. 3, respectively. It should be noted that the LO frequencies obtained in our experiment are not sensitive to the error in the absolute reflectivity and to the assumed in-plane conductivity, which is also fitted, while the TO frequencies depend on them both. However, this dependence is rather weak. In Table II we show our values of TO and LO frequencies in Bi2212, together with the values obtained by Tajima $et\ al.$[16] from the normal incidence reflectivity done on the ac plane at 6 K. In the latter case, the TO frequencies can be evaluated directly from the reflectivity spectrum. The LO frequencies are calculated via Kramers-Kronig transformation. From this comparison, one can see that the discrepancy between the LO frequency values obtained with the two different methods, on different samples, is only few wave numbers except for the highest-frequency mode, and that the TO values differ less than 10 cm^{-1}. This means that although we have a rather complicated situation, with the mixed ab-plane and c-axis response, we can get quite accurate values of the phonon parameters: transversal and longitudinal frequencies, and consequently, oscillator strength.

V. DISCUSSION

A body-centered-tetragonal structure $I4/mmm$ (D_{4h}^{17}) has been most frequently used in the interpretation of the infrared and Raman spectra of both bismuth and thallium cuprates. The unit cell for Tl$_2$Ba$_2$CuO$_6$ and Tl$_2$Ba$_2$CaCu$_2$O$_8$ is shown in Fig. 4. The structure of Bi$_2$Sr$_2$CuO$_6$ and
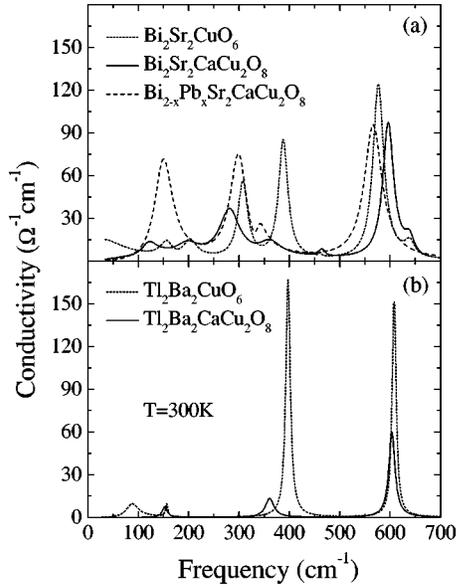
FIG. 2. The *c*-axis conductivity (a) for the Bi and (b) for Tl compounds, obtained from the fit of the reflectivity to the Drude-Lorentz model.

Bi₂Sr₂CaCu₂O₈ resembles the structure of the corresponding thallium compounds, where Bi and Sr substitute Tl and Ba, respectively. However, the crystal lattice of superconducting Bi cuprates has orthorhombic distortions, which lead to the doubled $\sqrt{2} \times \sqrt{2}$ unit cell in the *ab* plane. Moreover, there is a monoclinic incommensurate modulation of the structure with a period (4.5–5)**b**. The factor group analysis for the space group $I4/mmm$ predicts 5 A_{2u} out-of-plane and 6 E_u in-plane IR active modes for single-layer and $6A_{2u} + 7E_u$ for double-layer compounds, respectively. However, seven *c*-axis modes can be resolved in the case of Bi2201 and

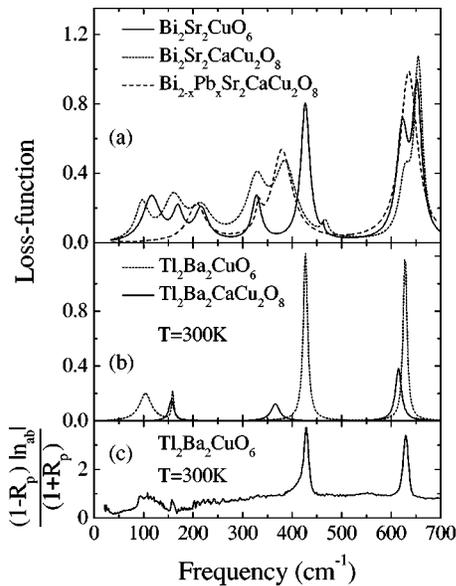
FIG. 3. The *c*-axis loss function (a) for the Bi and (b) for Tl compounds, obtained from the fit of the reflectivity to the Drude-Lorentz model. Shown in (c) is the experimentally measured $(1 - R_p)|n_{ab}|/(1 + R_p)$ function of Tl2201, which peaks at the longitudinal frequencies.
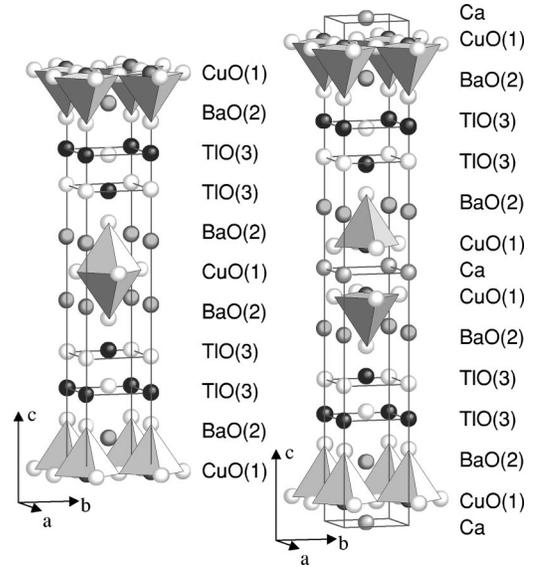

FIG. 4. Crystal structure of Tl₂Ba₂CuO₆ (left) and Tl₂Ba₂CaCu₂O₈ (right).

Bi2212 and only four modes are clearly seen in the case of Tl2201 and Tl2212 (Fig. 1). Extra phonon modes are present in the Bi spectra due to the lower symmetry. The six strongest *c*-axis modes are observed in the Bi2212 spectrum at 97, 174, 220, 328, 383, and 628 cm⁻¹. The last, 628 cm⁻¹, mode is split into main and satellite structures. The satellite at 655 cm⁻¹ and the two additional phonons at 469 and 472 cm⁻¹, which have very small optical strength and can be resolved only at low temperatures, seem to result from orthorhombic and monoclinic distortions. This implies that deviations from the basic $I4/mmm$ structure have some, but rather small effect on the phonon spectrum.

The lattice dynamical calculations for Tl2201, Tl2212, and Bi2212 were performed using the shell model[30,31] and the rigid-ion model.[49–51] The space group $I4/mmm$ was used in both cases. The assignments of the modes and the frequencies from the lattice dynamical calculation are given in Table III. TO frequencies were calculated in the rigid-ion model, and TO-LO splitting from the shell model. Although the shell model is a more powerful technique, it turns out that the eigenfrequencies and the character of the vibrations calculated in the rigid-ion model are often closer to the experimental data. However, the agreement is still not perfect. In our discussion, we will compare the the phonon frequencies with the calculated ones, but we will go beyond the $I4/mmm$ group when we discuss the modulation induced modes. From now on we will indicate the oxygen in the CuO planes as O(1), in the SrO (BaO) planes as O(2), and in the BiO (TlO) planes as O(3), as shown in Fig. 4.

A. Phonon modes

Let us consider first the high-frequency modes. They mainly involve motion of light oxygen ions. For simplicity we will discuss here the LO frequencies of the double-layer compounds. The corresponding frequencies for the single-layer compounds are given in Tables I and II, and the assignment of the oxygen modes is identical for both systems. The oxygen vibration modes in Tl (Bi) compounds are at

TABLE III. Calculated values of the c-axis phonon parameters.

This work ν_T	Prade et al.,[a] Kulkarni et al.[b] Assignment	$\tilde{\nu}_{T_j}$ ($\tilde{\nu}_{L_j}$)	Jia et al.[c] Assignment	$\tilde{\nu}_{T_j}$
		$Tl_2Ba_2CuO_6$		
78	Cu, Ba, Tl′	108 (108)	Cu, Tl′	146
157	Cu, Ba′	129 (143)	Cu, Tl, Ba′	160
386	O(1)	294 (341)	O(1), Ba′	376
	O(2), O(1)′	413 (451)	O(2), O(3), Tl′	537
603	O(3), O(2)′	602 (648)	O(3), O(2)′	568
		$Tl_2Ba_2CaCu_2O_8$		
	Cu, Ba, Tl′	108 (108)	Cu, Ba, Tl′	95
152	Cu, Ba′	113 (134)	Cu, Ba′	132
	O(1), Ca	210 (238)	O(1), Ca, Ba′	223
339	O(2), O(3), Ca′	355 (437)	Ca, Ba, O(1), O(2)	371
	O(2), O(1)′, Ca	457 (462)	O(2), O(3)	500
598	O(3), O(2)′	591 (630)	O(2), O(3)′	568
		$Bi_2Sr_2CaCu_2O_8$		
81				
157	Cu, Sr, Bi′	137 (141)	Cu, Sr, Bi′	164
198	Cu, Sr′	169 (169)	Cu, Sr′	225
301	O(1), Ca, Sr′	277 (278)	O(1), Ca, Sr′	281
357	O(3), Ca′	334 (477)	O(1), O(2)	442
(462)	O(1), O(3)′, Ca	487 (497)	O(2), O(3)	467
610	O(3), O(2)′	514 (530)	O(2), O(3)′	617

[a]Reference 30.
[b]Reference 31.
[c]References 49–51.

615 cm^{-1} (628/655 cm^{-1}), 366 cm^{-1} (383 cm^{-1}), and additionally at 328 cm^{-1} in the Bi compounds.

We assigned the highest-frequency mode, i.e., at 615 cm^{-1} (628/655 cm^{-1}), to the out-of-phase vibration of O(2) and O(3), in agreement with the lattice dynamical calculations, given in Table III. The splitting of this peak in Bi2201 and Bi2212, observable in Fig. 1(a), is due to the characteristic incommensurate modulation[52] of these compounds. This monoclinic superstructure is very often attributed to the incorporation of extra oxygen atoms in the BiO planes every 4.5–5 periods, although O(2) vacancies or element substitutions are also considered to explain the superstructure. The modulation period 4.5b on our Bi2212 sample was measured by low-energy electron diffraction (LEED).[53] Whatever the reason for the superstructure is, we use the fact that the modulation is not sinusoidal, but rather forms narrow stripes aligned along the a axis, as indicated by high-resolution electron microscopy[54] and x-ray detection of higher-order superstructure reflections. In this case, we can consider an oscillator model with every fifth oscillator slightly different as could be the case in presence of extra oxygen. Because there are four undisturbed and one disturbed cells in each supercell, the ratio of the optical strength of these two modes should be around 4, which is close to the ratio of 4.6 observed in Bi2212 (Table II). In Bi2201, the interaction within BiO layers is relatively stronger, due to the weaker perovskitelike CuO$_2$ block. The higher interaction

strength causes the redistribution of the spectral weight in favor of the stronger mode. The disappearance of the double structure in Pb-doped Bi2212 (see Fig. 1) supports this mode assignment. The substitution of 20% Bi^{3+} by Pb^{2+} relaxes the strong monoclinic superstructure distortion and induces a weaker orthorhombic modulation with a period at least twice as long.[55] No other mode shows such noticeable splitting. Taking into account that the most significant displacement of ions with respect to the tetragonal $I4/mmm$ structure occurs in the BiO planes and, thus, the modulation should mostly affect interatomic bonding in these layers, we gave the earlier mentioned assignment to this mode.

We ascribe the weak shallow structures between 500 and 600 cm^{-1} to in-plane phonons. The minimum at 508 cm^{-1} is also present in the ab-plane reflectivity of Bi2201, and it was reported as an in-plane phonon mode.[9] A similar observation seems to hold for the 560 cm^{-1} mode in Tl2201.[8] Small sharp minima around 470 cm^{-1} in Bi compounds are most probably zone-boundary modes, which become IR active due to the lattice distortion.

The next oxygen mode at 366 cm^{-1} in the Tl compound (383 cm^{-1} in Bi) is one of the strongest modes. It is the most noticeable feature of the spectra in Fig. 1 that this mode shifts up in frequency by 61 cm^{-1} in Tl and by 44 cm^{-1} in Bi cuprates, going from the double- to the single-layer compound. This shift indicates that this mode involves the motion of oxygen in CuO$_2$. In the shell model calculations[30,31] (Table III), the next predicted LO mode at 462 cm^{-1} in Tl2212, and at 497 cm^{-1} in Bi2212, is too weak and too high in frequency to be assigned to this vibration. The calculated mode eigenvector involves the motion of O(1) against O(2) and Ca. However, the compound without Ca should show a lower resonant frequency, as reported in Table III. The opposite behavior of this mode indicates that maybe the influence of Ca on this mode is not so strong. If we consider the next available candidates for the assignment in Table III, i.e., 294 cm^{-1} in Tl2201 and 355 cm^{-1} in Tl2212 modes, we again obtain the opposite frequency change from the single-layer 2201 to the double-layer 2212 compound. Thus, no mode predicted in lattice dynamical calculations could be ascribed to this phonon. Since the observed oscillator strength of this phonon is very high, we think that this mode involves mostly the in-phase motion of O(1) and O(2) against Cu.

The mode at 328 cm^{-1} is clearly seen only in the Bi compounds and it is present in both Bi2201 and Bi2212 at roughly the same frequency. In Tl2201, this mode also occurs at approximately the same frequency, but the optical strength is much weaker, and the line can be resolved only at a very low temperature. The 328 cm^{-1} mode in Tl2201 shows a narrowing with temperature, which is characteristic for c-axis phonon lines. Since the frequency of the 328 cm^{-1} mode in the Bi compounds does not vary with the number of CuO$_2$ layers, we conclude that it has O(2) and O(3) character. This phonon line is much broader than those at 427 cm^{-1} in Bi2201, and it resembles the modulation-induced splitting, which also supports the given assignment.

A weak structure is present in the Tl2201 spectrum around 230 cm^{-1}, and it could correspond to the 220 cm^{-1} mode in Bi compounds. The shape of this mode is tempera-

ture independent, which is the characteristic behavior of in-plane phonons. We therefore attribute this mode to an in-plane optical phonon.

The presence of the $328 \, \text{cm}^{-1}$ mode with c-axis polarization and the absence of the $220 \, \text{cm}^{-1}$ mode is in agreement with rigid-ion calculations[50,51] (see the $223 \, \text{cm}^{-1}$ mode of Tl2212 in Table III and the absence of its counterpart in Tl2201). However, these experimental results contradict the shell model calculations for Tl2201 (Table III),[31] where the $355 \, \text{cm}^{-1}$ mode is lacking.

The low-frequency modes are difficult to assign, since the heavy atoms involved in this kind of motion have comparable masses. The only mode that shifts with the change from the single to the double layer is the $114 \, \text{cm}^{-1}$ mode in Bi2201 ($98 \, \text{cm}^{-1}$ in Bi2212). The tendency to shift to a lower frequency is similar to those of the $383 \, \text{cm}^{-1}$ mode, and indicates that the motion of Cu atoms is involved. The other two phonons should include the Cu-O bending vibrations to minimize the interaction with Ca and, consequently, the motion of Bi, Sr, Tl, and Ba atoms to preserve the center of mass.

In all the compounds there exists a rather large discrepancy between lattice dynamical calculations and experiment, as shown in Table III: The calculations predict the additional mode of O(2)-O(3) character between 400 and $500 \, \text{cm}^{-1}$ with a rather large oscillator strength. Experimentally, this mode seems to be absent. Second, the mode with the largest TO-LO splitting is predicted to have lower frequency in Tl2201 ($294–341 \, \text{cm}^{-1}$ mode) than in Tl2212 ($355–437 \, \text{cm}^{-1}$ mode). The contradiction with the experiment can be readily observed in Fig. 1. A possible reason for this inconsistency is probably the fact that the early lattice dynamical calculations have been adjusted to data obtained on polycrystalline materials,[10–14] on which the in-plane and out-of-plane optical phonons cannot be separated. In fact, in Tl2223 and Bi2212 single crystals the in-plane phonons have been observed at $415 \, \text{cm}^{-1}$ and $420 \, \text{cm}^{-1}$, respectively.[56]

B. Resonances in intrinsic Josephson junctions

In the superconducting state the high-T_c compounds are considered to form a stack of superconducting CuO_2 planes separated by the nonsuperconducting heavy element rocksalt-type layers, where each pair of CuO_2 planes forms a Josephson junction. The interplane current showing typical Josephson behavior was observed in the I-V characteristics of thin mesoscopic structures of Bi2212 and Tl2223.[57] Subsequent measurements revealed a number of small intragap resonances on the resistive branch of the I-V curves.[32,33] The following investigations ruled out many known effects related to the superconducting energy gap or geometrical resonances. The I-V characteristic of a stack of junctions was shown to be a mere superposition of I-V curves of individual junctions,[58] which implies that all junctions are independent and that the intragap structures occur at characteristic bias voltages in every Josephson junction. Recently, Helm *et al.*[34] proposed that oscillations of the electric field within a junction, excited by the bias voltage due to the ac Josephson effect, couple to the IR active lattice vibrations and resonate at the longitudinal modes of the c-axis phonons. A comparison to the optical data was not done, because the resonances
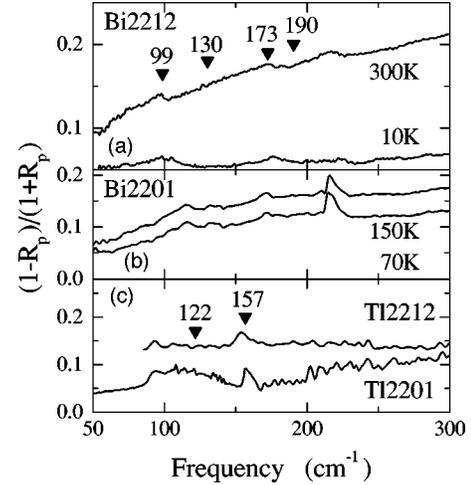

FIG. 5. Function $(1-R_p)/(1+R_p)$ for Bi2212 (a), Bi2201 (b), and Tl2212 and Tl2201 (c) for different temperatures in comparison with the positions of the resonances observed by the intrinsic Josephson junction spectroscopy: (a) for Bi2212 (marked by triangles and the corresponding value) and (c) for Tl2223.

lie well within the gap and the corresponding frequencies are difficult to access with presently available samples. Moreover, in the usual normal incidence technique, the longitudinal frequencies are obtained by Kramers-Kronig analysis and can be biased by noise and an error in absolute reflectivity at low frequencies.

In Fig. 5 the measured function $(1-R_p)/(1+R_p)$, where maxima correspond to the c-axis longitudinal frequencies, is shown for Bi2212 together with the positions of the four pronounced resonances observed in Ref. 58. In the superconducting state the phonon structure does not reveal substantial changes as can be seen from the 10 K curve. In the lower panel of Fig. 5, the optical data for Tl2201 and Tl2212 are compared to the tunnel data for Tl2223. Two phonons in the Bi2212 curve are in good agreement with the I-V resonances at 99 and $173 \, \text{cm}^{-1}$, and at least one coincides with the case of Tl2223. The latter phonon is observed in Tl2201 and Tl2212, but its position is almost unchanged in the systems with one and two CuO_2 layers per unit cell. We can expect that the third layer in Tl2223 should not substantially shift its frequency.

This agreement let us conclude that, as stated in the model of Helm *et al.*,[34] the optical phonons play the main role in the structure observed in the I-V characteristics. However, more resonances are observed in the tunneling experiment. The reason for this discrepancy between theory and experiment is that Helm *et al.*[34] consider the barrier filled with a macroscopic quantity of the material with properties similar to the bulk. In the following we will show that the additional resonances can correspond to zone-boundary modes, which are excited due to the nonuniform field distribution in the tunneling measurements. Indeed, the electric field E in the interlayer Josephson junction oscillates only between two adjacent CuO_2 planes and vanishes outside the junction. Thus, in the wave vector space, $E(q_c)$ spans the whole Brillouin zone following the Fraunhofer diffraction pattern. In optical measurements, the electromagnetic wave decays in the sample over the penetration depth length scale, which is much larger than the interplane distance. The corresponding
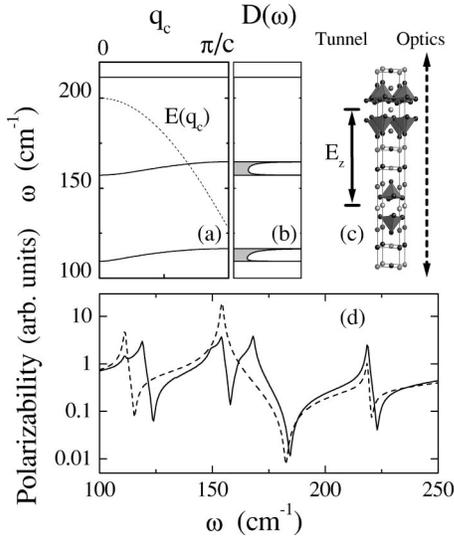
FIG. 6. (a) Simulated phonon dispersion of three branches in the low-frequency range for Bi2212 and q_c dispersion of the electric field in tunneling measurements. (b) The phonon density of states corresponding to the dispersion curves in (a). (c) Tunnel vs optics electric field distribution within the crystal. In the tunneling measurements, the electric field is localized within one junction. (d) Polarizability for the uniform (dashed line) and nonuniform (solid) electric field distribution, simulated on the stack of the ab planes, with each plane representing an atom in the unit cell.

distribution in q_c space is represented by the δ function near $q_c=0$. The electric field in the Josephson junction excites phonons for all q_c, and the induced polarization has peaks at the maxima of the phonon density of states. To illustrate this qualitatively we calculated the phonon dispersions for the three lowest-frequency modes using a reduced rigid-ion model. The curves are plotted in Fig. 6(a), together with the electric field distribution $E(q_c)$. For this calculation we represented each atom in the unit cell by a plane perpendicular to the c axis. The force constants, which include the nearest and next-nearest interactions in the unit cell, are adopted from the Ref. 49. The phonon density of states $D(\omega)$ is shown in Fig. 6(b). It can be seen that the polarization should peak at the zone-center and zone-boundary phonon frequencies. Figure 6(d) shows the frequency dependence of the polarization for the uniform field distribution (dashed curve) and for the nonuniform boxcar distribution (solid curve). In the latter case the electric field amplitude is finite (and constant) only within a single unit cell as shown in Fig. 6(c). To simulate this nonuniform field distribution, we extended our model to 1000 unit cells within the chain, with a finite dissipation introduced to avoid problems due to the circular boundary conditions. Figure 6(d) shows that the polarization indeed has maxima both at $\omega(q_c=0)$ and $\omega(\pi/c)$.

The zone-boundary phonons modes can become optically active if lattice distortions occur in the crystal structure. In Fig. 5 we plotted the data for Bi2201. The orthorhombic and monoclinic distortions of $I4/mmm$ structure are stronger in Bi2201 than in Bi2212, and this can explain why the $130\,\mathrm{cm}^{-1}$ mode is observed in the single-layer compound. It should be noted that the Raman-active modes could also be excited in the intrinsic Josephson junction measurements due to the strong ($\sim 10^5\,\mathrm{V/cm}$) polarization of the media by the dc bias voltage.

VI. CONCLUSION

We performed grazing incidence reflectivity measurements on bismuth and thallium superconducting cuprates. The technique was shown to permit accurate determination of the c-axis longitudinal frequencies. We fitted spectra with the Drude-Lorentz model and showed that the values of the phonon parameters agree with those obtained in normal incidence measurements. Therefore, we argue that the grazing incidence technique is an excellent tool for probing the c-axis properties in high-T_c superconductors on samples with a small size in the c direction, which is often a problem in normal incidence measurements.

We compared the c-axis TO and LO phonon frequencies in five structurally similar compounds $Tl_2Ba_2CuO_6$, $Tl_2Ba_2CaCu_2O_8$, $Bi_2Sr_2CuO_6$, $Bi_2Sr_2CaCu_2O_8$, and $Bi_{2-x}Pb_xSr_2CaCu_2O_8$ with lattice dynamical calculations and proposed an assignment for the main oxygen modes. The major difference is the assignment of the $366\,\mathrm{cm}^{-1}$ mode in 2212 compounds, which we consider to be the in-phase motion of O(1) and O(2) against Cu. We observed a substantial discrepancy between the available lattice dynamical calculations and our experimental data: The calculations predict a phonon mode between 400 and $500\,\mathrm{cm}^{-1}$, which we do not observe. Shell model calculations indicate that the oxygen mode with the largest TO-LO splitting in the double-layer 2212 compounds should be higher in frequency than those in the single-layer 2201 compounds, which is again inconsistent with our data.

The comparison of the LO frequencies obtained by our method with those inferred from intrinsic Josephson effect measurements shows that the latter technique—due to the nonuniform electric field distribution—is sensitive both to zone-center and zone-boundary phonons.

[1] A. P. Litvinchuk, C. Thomsen, and M. Cardona, in *Physical Properties of High-Temperature Superconductors IV*, edited by D. M. Ginsberg (World Scientific, Singapore, 1992), pp. 375–470.

[2] J. Schützmann, S. Tajima, S. Miyamoto, Y. Sato, and R. Hauff, Phys. Rev. B **52**, 13 665 (1995).

[3] C. C. Homes, T. Timusk, D. A. Bonn, R. Liang, and W. N. Hardy, Can. J. Phys. **73**, 663 (1995).

[4] J. H. Kim, H. S. Somal, M. T. Czyzyk, D. van der Marel, A. Wittlin, A. M. Gerrits, V. H. M. Duijn, N. T. Hien, and A. A.Menovsky, Physica C **247**, 297 (1995).

[5] R. Henn, A. Wittlin, M. Cardona, and S. Uchida, Phys. Rev. B **56**, 6295 (1997).

[6] A. M. Zibold, D. B. Tanner, and H. Berger, Physica B **244**, 27 (1998).

[7] I. Terasaki, S. Tajima, H. Eisaki, H. Takagi, K. Uchinokura, and S. Uchida, Phys. Rev. B **41**, 865 (1990).

[8] A. V. Puchkov, T. Timusk, S. Doyle, and A. M. Hermann, Phys. Rev. B **51**, 3312 (1995).

[9] A. A. Tsvetkov, J. Schützmann, J. I. Gorina, G. A. Kaljusnaia, and D. van der Marel, Phys. Rev. B **55**, 14 152 (1997).

[10] Z. V. Popović, C. Thomsen, M. Cardona, R. Liu, G. Stanišić, R. Kremer, and W. Köning, Solid State Commun. **66**, 965 (1988).

[11] C. M. Foster, K. F. Voss, T. W. Hagler, D. Mihajlović, and A. J. Heeger, Solid State Commun. **76**, 651 (1990).

[12] T. Zetterer, M. Frantz, J. Schützmann, W. Ose, H. H. Otto, and K. F. Renk, Phys. Rev. B **41**, 9499 (1990).

[13] K. Kamarás, S. L. Herr, C. D. Porter, D. B. Tanner, S. Etemad, and J. M. Tarascon, Phys. Rev. B **43**, 11 381 (1991).

[14] D. Mihajlović, T. Martelj, K. F. Voss, A. J. Heeger, and N. Herron, Phys. Rev. B **45**, 8016 (1992).

[15] A. M. Zibold, M. Dürrler, A. Gaymann, H. P. Geserich, N. Nücker, V. M. Burlakov, and P. Müller, Physica C **193**, 171 (1992).

[16] S. Tajima, G. D. Gu, S. Miyamoto, A. Odagawa, and N. Koshizuka, Phys. Rev. B **48**, 16 164 (1993).

[17] J. H. Kim, B. J. Feenstra, H. S. Somal, D. van der Marel, W. Y. Lee, A. M. Gerrits, and A. Wittlin, Phys. Rev. B **49**, 13 065 (1994).

[18] L. V. Gasparov, O. V. Misochko, M. I. Eremets, E. S. Itskevich, A. V. Lomsadze, V. V. Struzhkin, and A. M. Shirokov, Solid State Commun. **72**, 465 (1989).

[19] M. Käll, L. Börjesson, M. Kakihana, C. Ström, L.-G. Johansson, S.-G. Eriksson, and T. Larsson, Physica C **185-189**, 821 (1991).

[20] R. Liu, M. V. Klein, P. D. Han, and D. A. Payne, Phys. Rev. B **45**, 7392 (1992).

[21] R. Nemetschek, O. V. Misochko, B. Stadlober, and R. Hackl, Phys. Rev. B **47**, 3450 (1993).

[22] M. Käll, L. Börjesson, C. Ström, S. Eriksson, and T. Larsson, Physica C **220**, 131 (1994).

[23] M. C. Krantz, I. I. Mazin, D. H. Leach, W. Y. Lee, and M. Cardona, Phys. Rev. B **51**, 5949 (1995).

[24] M. Kakihana, M. Osada, M. Käll, L. Börjesson, H. Mazaki, and H. Yasuoka, Phys. Rev. B **53**, 11 796 (1996).

[25] M. Kang, G. Blumberg, M. V. Klein, and N. N. Kolesnikov, Phys. Rev. B **56**, R11 427 (1997).

[26] C. Kendziora, S. B. Quadri, and E. Skelton, Phys. Rev. B **56**, 14 717 (1997).

[27] A. A. Martin, J. A. Sanjurjo, K. C. Hewitt, X-Z Wang, J. C. Irwin, and M. J. G. Lee, Phys. Rev. B **56**, 8426 (1997).

[28] M. Osada, M. Kakihana, M. Käll, and L. Börjesson, Phys. Rev. B **56**, 2847 (1997).

[29] X. H. Chen, M. Yu, G. G. Qian, Z. S. Liu, L. Z. Cao, J. Zou, and C. Y. Xu, Phys. Rev. B **57**, 5082 (1998).

[30] J. Prade, A. D. Kulkarni, F. W. Wette, U. Schröder, and W. Kress, Phys. Rev. B **39**, 2771 (1989).

[31] A. D. Kulkarni, F. W. Wette, J. Prade, U. Schröder, and W. Kress, Phys. Rev. B **41**, 6409 (1990).

[32] K. Schlenga, G. Hechtfisher, R. Kleiner, W. Walkenhorst, P. Müller, H. L. Johnson, M. Veith, W. Brodkorb, and E. Steinbeiß, Phys. Rev. Lett. **76**, 4943 (1996).

[33] A. Yurgens, D. Winkler, N. Zavaritsky, and T. Claeson, Proc. SPIE **2697**, 433 (1996).

[34] Ch. Helm, Ch. Preis, F. Fosthofer, J. Keller, K. Schlenga, R. Kleiner, and P. Müller, Phys. Rev. Lett. **79**, 737 (1997).

[35] J. I. Gorina, G. A. Kaljujnaia, V. I. Ktitorov, V. P. Martovitsky, V. V. Rodin, V. A. Stepanov, A. A. Tsvetkov, and S. I. Vedeneev, Solid State Commun. **85**, 695 (1993).

[36] J. I. Gorina, G. A. Kaljushnaia, V. I. Ktitorov, V. P. Martovitsky, V. V. Rodin, V. A. Stepanov, and S. I. Vedeneev, Solid State Commun. **91**, 615 (1994).

[37] V. P. Martovitsky, J. I. Gorina, and G. A. Kaljushnaia, Solid State Commun. **96**, 893 (1995).

[38] T. W. Li, P. H. Kes, N. T. Hien, J. J. M. Franse, and A. A. Menovsky, J. Cryst. Growth **135**, 481 (1994).

[39] N. N. Kolesnikov, V. E. Korotkov, M. P. Kulakov, R. P. Shibaeva, V. N. Molchanov, R. A. Tamazyan, and V. I. Simonov, Physica C **195**, 219 (1992).

[40] N. N. Kolesnikov, M. P. Kulakov, V. N. Molchanov, I. F. Schegolev, R. P. Shibaeva, V. I. Simonov, R. A. Tamazyan, and O. M. Vyasilev, Physica C **242**, 385 (1995).

[41] C. A. Wang, Z. F. Ren, J. H. Wang, D. K. Petrov, M. J. Naughton, W. Y. Yu, and A. Petrou, Physica C **262**, 98 (1996).

[42] Z. F. Ren, J. H. Wang, and D. J. Miller, Appl. Phys. Lett. **69**, 1798 (1996).

[43] M. M. Eddy, U.S. Patent Nos. 5,476,836 (1995), and 5,508,255 (1996).

[44] B. A. Willemsen, K. E. Kihlstrom, T. Dahm, D. J. Scalapino, B. Gowe, D. A. Bonn, and W. N. Hardy, Phys. Rev. B **58**, 6650 (1998).

[45] J. Schützmann, H. S. Somal, A. A. Tsvetkov, D. van der Marel, G. E. J. Koops, N. Koleshnikov, Z. F. Ren, J. H. Wang, and E. Brück, Phys. Rev. B **55**, 11 118 (1997).

[46] A. A. Tsvetkov, D. van der Marel, K. A. Moler, J. R. Kirtley, J. L. de Boer, A. Meetsma, Z. F. Ren, N. Koleshnikov, D. Dulic, A. Damascelli, M. Grüninger, J. Schützmann, J. W. van der Eb, H. S. Somal, and J. H. Wang, Nature (London) **395**, 360 (1998).

[47] D. van der Marel, H. S. Somal, J. W. van der Eb, and J. Schützmann, in *Proceedings of the 10th Anniversary HTS Workshop on Physics, Materials and Applications*, Houston, Texas, 1996, edited by B. Batlogg, C. W. Chu, W. K. Chu, D. U. Gubser, and K. A. Müller (World Scientific, Singapore, 1996), pp. 357–360.

[48] A. A. Tsvetkov, D. van der Marel, D. Dulić, H. J. Molegraaf, N. N. Kolesnikov, B. Willemsen, and Z. F. Ren, in *Superconducting Superlattices II: Native and Artificial*, edited by I. Bozovic and D. Pavuna [Proc. SPIE **3480**, 2 (1998)].

[49] C. S. Jia and S. W. Zhou, Phys. Status Solidi A **163**, K49 (1991).

[50] C. S. Jia, J. Xiaowei, C. Puchun, D. Shier, and X. Yang, Chin. J. Low Temp. Phys. **17**, 305 (1995).

[51] C. S. Jia, P. Y. Lin, Y. Xiao, X. W. Jiang, X. Y. Gou, S. Huo, H. Li, and Q. B. Yang, Physica C **268**, 41 (1996).

[52] R. M. Hazen, in *Physical Properties of High-Temperature Superconductors II*, edited by D. M. Ginsberg (World Scientific, Singapore, 1992), pp. 121–198.

[53] K. Schulte (unpublished).

[54] A. I. Beskrovnyi, S. Durčok, J. Hejtmánek, Z. Jirák, E. Pollert, and I. G. Shelkova, Physica C **222**, 375 (1994).

[55] Mao Zhiqiang, Fan Chenggao, Shi Lei, Yao Zhen, Yang Li, Wang Yu, and Zhang Yuheng, Phys. Rev. B **47**, 14 467 (1993).

[56] M. Shimada, K. Mizuno, S. Miyamoto, M. Shimizu, and J. Tanaka, Physica C **193**, 353 (1992).

[57] R. Kleiner, F. Steinmeyer, G. Kunkel, and P. Müller, Phys. Rev. Lett. **68**, 2394 (1992).

[58] K. Schlenga, R. Kleiner, G. Hechtfischer, M. Mößle, S. Schmitt, P. Müller, C. Helm, C. Preis, F. Forsthofer, J. Keller, H. J. Johnson, M. Veith, and E. Steinbeiß, Phys. Rev. B **57**, 14 518 (1998).